COMMISSIONING OF EXPERIMENTAL FACILITY FOR OIL CIRCULATION RATE MEASUREMENTS IN A VAPOR COMPRESSION SYSTEM

BY

SYED ANGKAN HAIDER

THESIS

Submitted in partial fulfillment of the requirements
for the degree of Master of Science in Mechanical Engineering
in the Graduate College of the
University of Illinois Urbana-Champaign, 2023

Urbana, Illinois

Advisor:

Professor Nenad Miljkovic

ABSTRACT

Lubricant oil is essential in typical vapor compression refrigeration and air conditioning systems, where the oil is primarily used to lubricate the moving parts inside the compressor. The relative motion between the moving parts can cause them to wear out and eventually lead to the failure of the compressor. So, the oil helps to extend the useful life of the compressor. In addition to that, the oil has other benefits such as dissipating heat away from the compressor and ensuring better sealing and hence good volumetric efficiency.

Outside the compressor, the oil is a contaminant and has little use, and mostly causes problems at both the system and component levels. Oil is known to generally reduce heat transfer coefficient and increase pressure drop. It can coat the tube inner walls and act as a barrier to heat transfer by reducing the area available for heat transfer and presenting itself as an additional thermal resistance. As a result, both the system capacity and coefficient of performance drop (COP), and energy efficiency takes a hit. The movement of oil from the compressor to the rest of the system and back to the compressor is known as oil circulation. However, not all the oil returns to the compressor and some gets stuck at different locations around the system in a process called oil retention. To understand the oil effects better, a better knowledge of the degree of oil circulation is necessary. The oil motion around the system is quantified by the oil circulation rate (OCR) which is the ratio of the oil flow rate to the total flow rate of the oil-refrigerant mixture. In real systems, the ASHRAE standard 41.4 is used to measure OCR in steady state. This method involves taking a sample of refrigerant-oil mixture from a system running in steady state. Once the sample is taken, mass analysis of the sample is done to determine the oil concentration at the outlet of the condenser. The oil concentration is the same as the oil circulation rate since the mixture is miscible and is a homogeneous liquid.

The present work was aimed at building and commissioning an experimental facility that could be used to run such tests. The whole facility was not built from scratch, a lot of the components were present in the lab, and our job was to build and modify the facility for the tests we wanted to perform. This included finding the current components, connecting everything, calibrating all the sensors, fixing the data logging unit, and all the other crucial tasks needed to have an experimental facility that would cater to all our needs. The next goal was to learn how to run the experimental facility at specified standard indoor and outdoor conditions to provide us with comparable test results. Finally, once steady state system conditions were achieved, oil circulation rate was measured for different compressor speeds to see the variation in oil circulation around the system.

ACKNOWLEDGMENTS

I want to convey my sincerest appreciation to my advisor, Professor Nenad Miljkovic, who was and still is a guiding force and mentor for me. He has not only provided unwavering support but has also been a friend, instilling in me a commitment to honest research that will undoubtedly influence my future career. Special thanks to Professor Stefan Elbel, who introduced me to the world of HVAC&R and taught me how to conduct independent research. The immense enthusiasm and passion for his work was contagious, and I am sure that I will be able to put all his teachings to good use.

I am thankful for the camaraderie and intellectual exchange with my colleagues at the Air Conditioning and Refrigeration Center. A heartfelt thank you to Jun, Toki, Min, Yingyue, Minwoong, Purav, Haider, Muntasir, and others who welcomed me into the academic community and provided invaluable help and support at every step. Special thanks to Xin for welcoming me into the lab, helping with everything including building the experimental facility, planning our research, proofreading my work, and so much more.

I would be remiss not to express my profound gratitude to my friends who were an integral part of my journey. Partha, Kazi and Asif, were there since the early days and they stood by me through thick and thin. Special thanks to Sugun and Tanveer for always offering candid advice, for their willingness to offer a helping hand whenever necessary and for accompanying me through some of the toughest moments. Thanks also to Shuvra, for being a constant source of encouragement, and for bolstering me during some very challenging times.

Finally, heartfelt thanks go to my family, for their love, inspiration, and unwavering belief in my potential.

To my parents, for their unwavering support and encouragement.

TABLE OF CONTENTS

NOMENCLATURE vii

CHAPTER 1: INTRODUCTION 1
1.1 Basic concepts and literature review 1
1.2 Objectives 4

CHAPTER 2: EXPERIMENTAL FACILITY 5
2.1 Details of different components 5
2.1.1 Compressor 5
2.1.2 Condenser and evaporator 7
2.1.3 Expansion device 9
2.2 The full experimental setup 10
2.3 Flow visualization at compressor discharge 13

CHAPTER 3: OCR MEASUREMENT AT LIQUID LINE 14

CHAPTER 4: RESULTS 16
4.1 Steady state data 16
4.2 OCR measurements 26
4.3 Flow visualization at compressor discharge 29

CHAPTER 5: CONCLUSIONS 32

REFERENCES 34

APPENDIX A: EES CODE FOR SAMPLE SYSTEM CALCULATIONS 38

APPENDIX B: P-H DIAGRAM FOR SYSTEM IN STEADY STATE 40

NOMENCLATURE

Abbreviations	
OCR	oil circulation rate
COP	coefficient of performance
EEV	electronic expansion valve
HVAC&R	heating, ventilation, and air conditioning & refrigeration
PAG	polyalkylene glycol

Variables	
$\dot{m}_{oil}$	mass flow rate of oil
$\dot{m}_{ref}$	mass flow rate of refrigerant
m_{oil}	mass of oil in sampling cylinder
m_{ref}	mass of refrigerant in sampling cylinder
M_1	mass of only sampling cylinder
M_2	mass of sampling cylinder and refrigerant-oil mixture
M_3	mass of sampling cylinder and oil only
T	temperature
P	pressure
DP	differential pressure
M_r	system mass flow rate measured by mass flow meter at condenser outlet

Subscripts	
r, ref	refrigerant
o	oil
cpro	compressor refrigerant outlet
cri	condenser refrigerant inlet
cro	condenser refrigerant outlet
eri	evaporator refrigerant inlet
ero	evaporator refrigerant outlet
cai	condenser air inlet
cao	condenser air outlet
cn	condenser nozzle
eai	evaporator air inlet
eao	evaporator air outlet
en	evaporator nozzle
avg	average

CHAPTER 1: INTRODUCTION

1.1 Basic concepts and literature review

In vapor compression refrigeration and air conditioning (AC) systems, the key components are the compressor, condenser, expansion device and the evaporator. In such systems, the compressor is considered to be the "heart" of the system since it is what really runs the refrigeration cycle and maintains the proper functionality of the system. Some of the key functions of the compressor include circulation of the refrigerant around the refrigeration loop, compression and subsequent increase of temperature and pressure of the flowing refrigerant, maintaining the flow, providing mechanical work, and ensuring good overall system efficiency.

Since the compression process occurring inside the compressor involves relative motion of different moving parts sliding against each other, the parts are subjected to frictional wear and tear. To help reduce this wear and tear, lubricant oils are added to the compressor to coat the moving parts, thus reducing the detrimental effects of friction, and extending the useful life of the compressor. Additionally, the oil helps to dissipate heat away from the compressor and has a sealing effect which ensures good volumetric efficiency. So, considering the compressor at component level, the oil has some positive effects. However, the story is very different when the effects of oil at the system level are considered.

Even though the oil is added exclusively for the lubrication of the compressor, the oil, mixed with refrigerant, can leave the compressor (Figure 1.1), and circulate the entire system or get retained at certain locations, while some of it returns to the compressor too. Outside the compressor, the oil is a contaminant, and has several detrimental effects on the rest of the vapor compression system. Especially, at the heat exchangers, the oil film adds an extra layer of thermal

resistance due to the relatively poor thermal conductivity of oil. Oil on tube walls affects the boundary layer, causing the viscous sublayer to form and result in a more laminar flow which gives reduced convective heat transfer. The oil alters the properties of pure refrigerant, and can negatively impact the flow regimes, as shown by Wang *et al.* [1]–[4]. Flow regimes are closely related to heat transfer. In general, the oil reduces the heat transfer coefficient and increases pressure drop in the system.

In HVAC&R systems, the oil has two broad effects, namely, oil circulation and oil retention. Xu and Hrnjak [5] differentiated between the two by defining oil retention as the amount of oil that stays in a specific section of the pipeline or heat exchanger. It has the same unit as mass and is a static parameter describing how much oil gets accumulated in a certain location in the system. They described the oil circulation as the dynamic amount of oil flow circulated in the system. While oil retention is different in different locations of the system, the oil circulation is the same everywhere since it is related to the mass flow rate. The focus of the present work was on oil circulation, and the parameter used to quantify the oil circulation in the system is called oil circulation rate (OCR). The OCR is defined as the ratio of the flow rate of oil to the total flow rate of the mixture of oil and refrigerant that flows through the system. Equation (1.1) gives the equation for the calculation of OCR.

$$OCR = \frac{\dot{m}_{oil}}{\dot{m}_{oil} + \dot{m}_{ref}} \tag{1.1}$$

Radermacher *et al.* [6], Youbi-Idrissi and Bonjour [7] and several other researchers investigated the effect of OCR on the system, and the consensus was that at high OCRs, the amount of oil accumulated in the evaporator increases and the area available for heat transfer decreases. So, the heat transfer coefficient takes a hit. The review article of Shen and Groll [8] also showed that most studies reported that more oil in the system results in increased pressure drops during

evaporation and condensation. Liu and Hrnjak [9] performed system level studies where they found that for a mobile AC system, both the system capacity and COP drop with the increase of OCR.

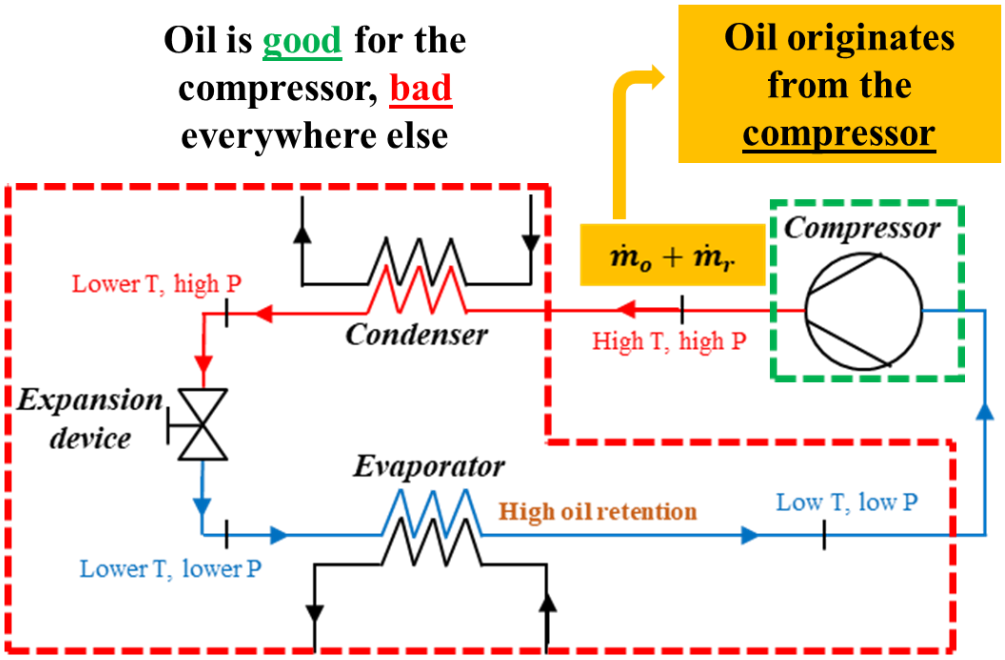

Figure 1.1: Oil in a typical vapor compression system

With all the negative effects of oil, both at the system and the component levels, there has been a recent industry shift towards low OCR compressors, and with the OCR values of interest getting smaller and smaller, it has become increasingly important to be able to measure OCR accurately and repeatably. There are a number of different OCR measurement techniques available, but all methods of OCR measurement are calibrated using the ASHRAE standard 41.4 (2015). This standard describes OCR measurement by taking a liquid sample of refrigerant-oil mixture from the condenser outlet (liquid line) of the system by using an evacuated type sampling cylinder, and then performing gravimetric analysis to measure the oil concentration in the sample.

If the refrigerant-oil mixture is a miscible combination in the liquid phase, then it will form a homogeneous mixture and the concentration will ideally be the same as the OCR. Haider *et al.* [10]–[13] showed that the best method to measure OCR experimentally was to use a flow-through type sampling cylinder rather than the evacuated-type prescribed in the ASHRAE standard. They explained how the flow-through cylinder avoids all the possible problems involved in the flashing flows that arise for the evacuated sampling cylinder during the filling process. For the present work, flow-through sampling was performed for all OCR measurements.

1.2 Objectives

The main objective of the work performed for this thesis was to prepare an experimental facility that could emulate a real automotive air conditioning system. The goal was to first prepare the facility for running AC tests, and this included installing the compressor, connecting the different components (condenser, evaporator, etc.), charging refrigerant and lubricant, installing transparent tube sections for flow visualization, running tests at specified standard conditions, learning how to get steady-state data, and finally measuring the OCR in the system at different compressor speeds.

CHAPTER 2: EXPERIMENTAL FACILITY

2.1 Details of different components

As mentioned before, the main components of a vapor compression system include a compressor, condenser, expansion device and evaporator. Table 2.1 gives the summary of the different components used in the experimental facility.

Table 2.1: The four main components

Compressor	Variable displacement swash plate type (variable speed)
Condenser	Microchannel type
Expansion device	Electronic expansion valve (EEV)
Evaporator	Microchannel type

2.1.1 Compressor

The present study used a variable speed compressor, and the specific type used was a variable displacement swash plate compressor. The idea was to investigate the oil circulation and pertaining effects at different compressor speeds. Inampudi *et al.* [14]–[17] compared different compressor capacity modulation strategies using experiments, modeling and concluded that the variable speed compressors have the best seasonal performance. Their system level study also showed that better heat exchanger performance could overcome a higher efficiency compressor.

Inampudi and Elbel, during their charge optimization study in an R410A system with condenser, receiver and dedicated subcooler, found that peak in COP occurs when the receiver is empty for cooling application and operating at this peak charge improved the seasonal performance of a variable speed compressor [18].

The basic working principle of a swash plate compressor is widely known, and is nicely summed up in the numerical works of Tian *et al.* [19]. They described how a variable displacement swash plate compressor has a main shaft, a drive rotor, a swash plate and pistons. The drive rotor remains fixed in the main shaft and it drives the swash plate rotating along with the main shaft. The swash plate converts its rotary motion into linear reciprocation of the pistons through the sliding shoes inside the pistons. A schematic of the swash plate compressor from their work is shown in Figure 2.1.

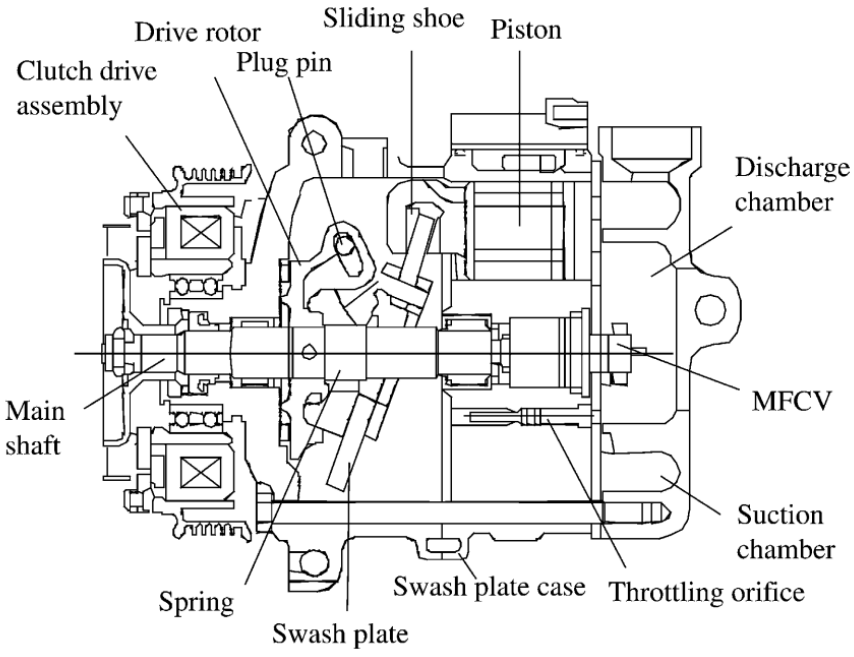

Figure 2.1: Schematic of typical swash plate compressor, taken from [15]

The degree of oil circulation, i.e., the OCR, depends on the compression suction and discharge pressures, and hence the compressor speeds too. The swash plate compressor used was a Denso 10PA17C compressor that is typically used for automotive air conditioning applications. It was run using a pulley system that used a motor and a belt. The motor was controlled using a variable frequency drive (VFD). Photos of the motor and compressor are provided in Figure 2.2.

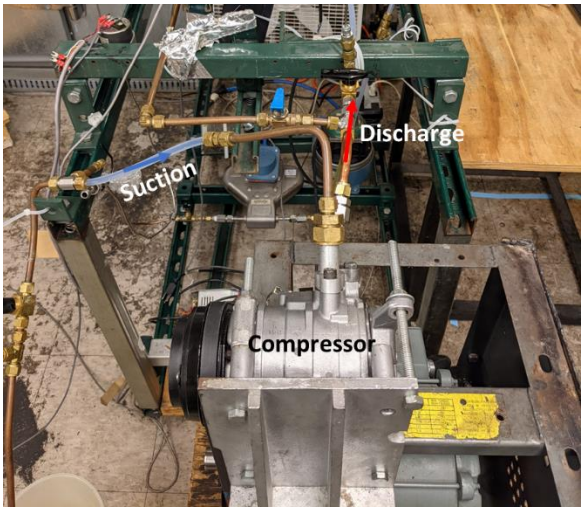

(a) The suction and discharge tubes of the compressor

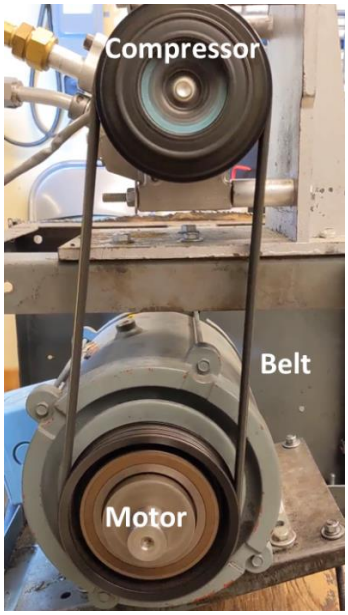

(a) Motor, compressor and belt

Figure 2.2: Photos of the compressor from the experimental facility

2.1.2 Condenser and evaporator

Both heat exchangers, i.e., the condenser and the evaporator, were microchannel type. The oil has a detrimental effect on both heat transfer coefficient and pressure drop for microchannel heat exchangers as investigated by Kim and Hrnjak [20], Li and Hrnjak [21], Zhu *et al.* [22] and

several others. So, that is the type investigated for the present work since the oil effects would be magnified.

Microchannel heat exchangers are simply variations of fin and tube heat exchangers. For the present case, the refrigerant flows through the enclosed channels (hydraulic diameter less than 1 mm) while air flows through connected fins in cross-flow. The key advantage of such types of heat exchangers is the fact that they provide greater surface area for heat transfer at the channel wall for the same volume. With the increased surface area, the energy efficiencies are higher due to improved heat transfer. Also, with the narrow channels, the amount of bulk fluid flowing is less, meaning that the heat transfer is less convection dominant, thus requiring less refrigerant charge for the same degree of heat transfer. Siddiqui [23] gave a nice schematic of a microchannel heat exchanger, shown in Figure 2.3.

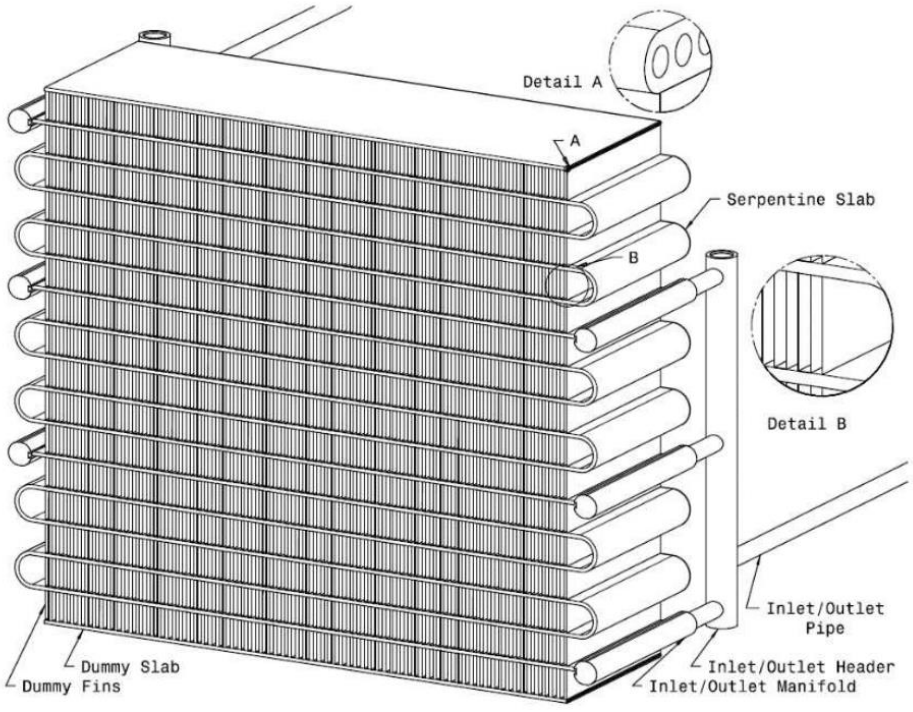

Figure 2.3: Schematic of a microchannel heat exchanger, taken from [19]

Photos of the condenser and the evaporator, both of which are microchannel type heat exchangers, used in our experimental facility are provided in Figure 2.4. Both heat exchangers were placed in a wind tunnel run with blowers. The blowers helped speed up steady state flow of air in the wind tunnels. Heaters and cooling water loops were available to set the desired air temperatures. Thermocouples and pressure sensors were available for measurement of temperature and air side pressure drop.

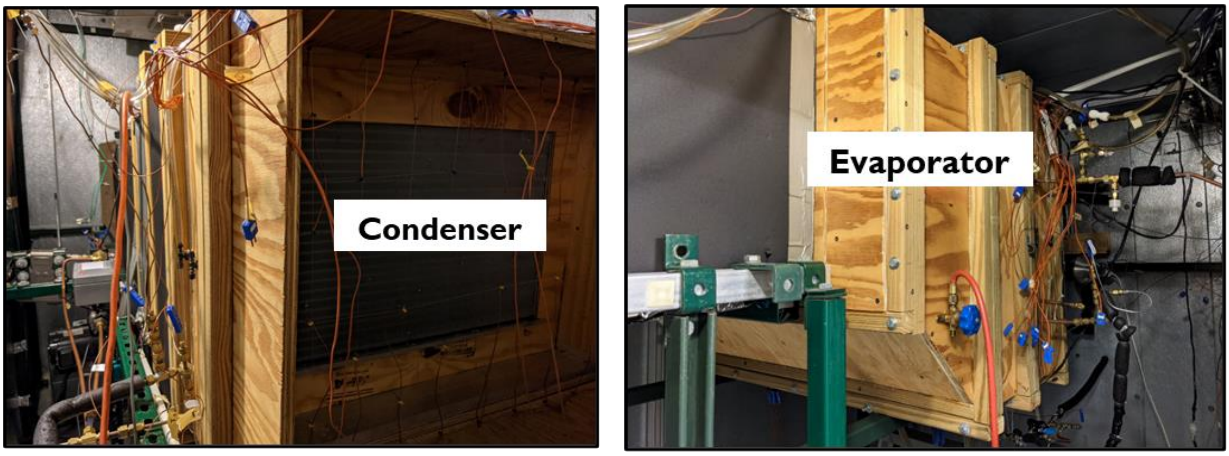

(a) Condenser room (b) Evaporator room

Figure 2.4: Photos of the condenser and evaporator from the experimental facility

2.1.3 Expansion device

The expansion device used in the current experimental facility was an electronic expansion valve (EEV). The EEV is placed between the condenser and the evaporator in a conventional vapor compression system to throttle the flow. It works like any valve, and in turn controls the flow of refrigerant through it. In an EEV, electronic signals are sent to it via a controller, and the signals cause a stepper motor inside the EEV to move a fraction of the revolution, depending on the electronic signal sent to the motor. A gear train drives the stepper motor, and it moves a pin at the

port, thus controlling the refrigerant flow through it. A thermistor and pressure sensor have to be installed at the evaporator outlet to sense the amount of EEV opening needed to obtain the required degree of superheat. The EEV used had two modes, namely, automatic and manual. The automatic mode allowed us to set a desired superheat, which automatically sets the correct EEV open ratio after monitoring the temperature and pressure readings from the thermistor and pressure sensor. The manual mode allowed us to set a desired EEV open ratio. Tests were run in both modes. Photos of the EEV, thermistor, pressure sensor and controller used in the experimental facility are provided in Figure 2.5.

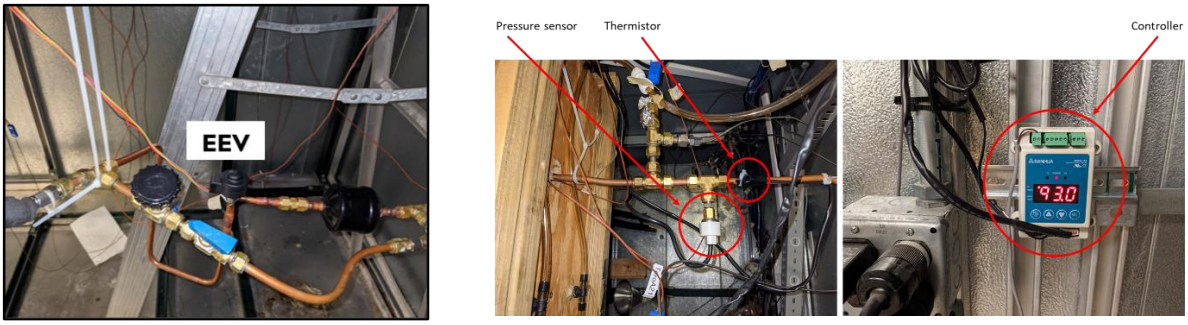

(a) EEV

(b) Thermistor, pressure sensor and controller

Figure 2.5: Photos of EEV, thermistor, pressure sensor and controller from the experimental facility

2.2 The full experimental setup

A schematic diagram of the experimental facility is provided in Figure 2.6. Figure 2.7 gives photos of the different components of the facility and how they are connected together. The temperatures inside the environmental chambers were maintained at the A_{Full} conditions as prescribed in AHRI Standard 210/240 (2020), with the outdoor temperature (condenser air-side temperature) at 95°F (35°C) and the indoor temperature (evaporator air-side temperature) at 80°F

(26.7°C). Both the condenser and the evaporator are placed inside environmental chambers, and heaters, blowers, and cooling water circuit are available inside the environmental chambers to ensure that the desired conditions can be achieved at steady-state condition.

The refrigerant used for the study was R134a, and the lubricant was PAG ISO 46 oil. This is a miscible combination of oil and refrigerant at the liquid line in the conditions of interest, and such a combination is expected to provide samples which are representative of the system. The total refrigerant charge added to the system was 2.2 kg, and 130 cm^3 of PAG ISO 46 oil was added to the suction side of the compressor as prescribed by the compressor manufacturer. The refrigerant charge added is higher than that added to conventional automotive vehicles since the system used for the study was larger with much longer lines, especially at the condenser outlet, where a lot of liquid refrigerant is present.

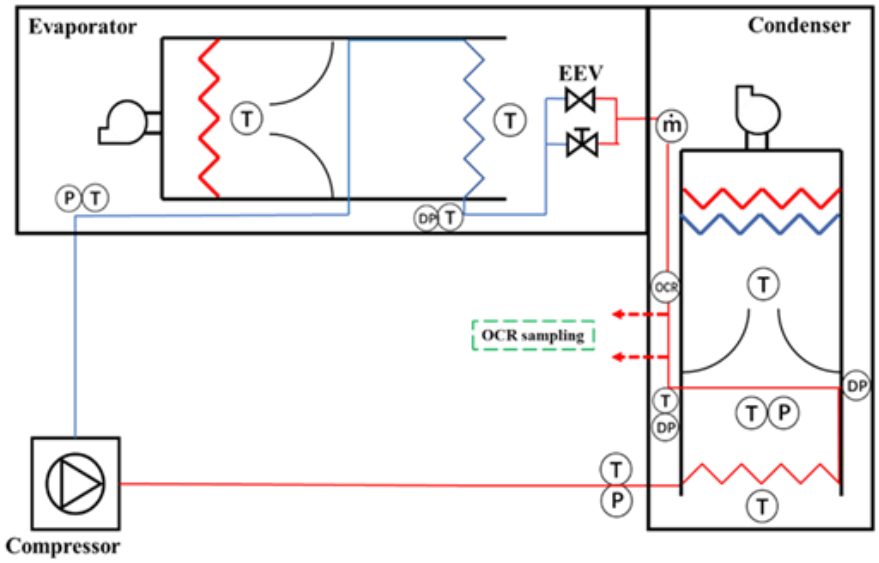

Figure 2.6: Schematic of experimental facility

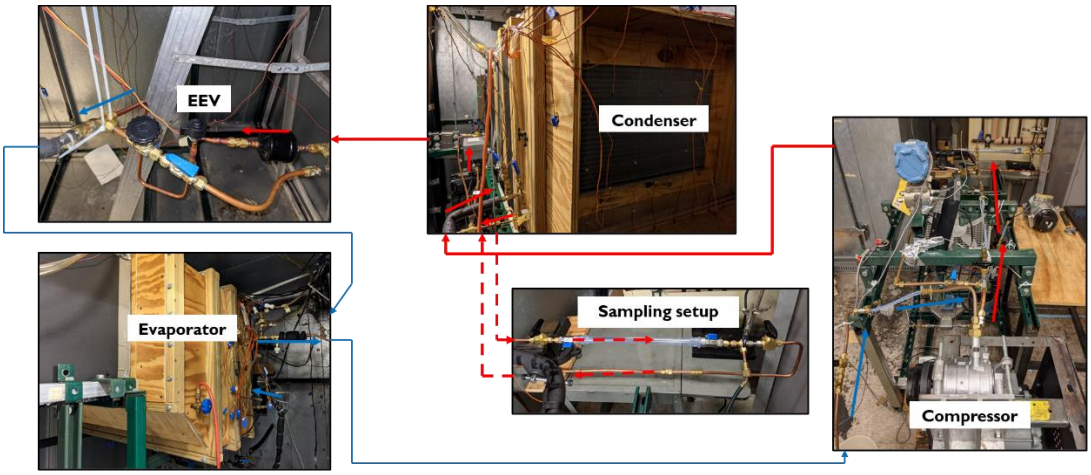

Figure 2.7: Different components of the experimental facility

The pressure, temperature, mass flow, etc. data are collected and transferred to a data-logger, which then sends the data to a VEE software that provides the real-time values and graphs. The software has a recording feature with an interval of 5 seconds. At steady-state condition, the recorded data are time averaged. Properties of refrigerants and other fluids are calculated using REFPROP 10.0.

To measure properties of the different flows, different sensors were installed at different locations of the system. The different sensors used are given in Table 2.2. The uncertainties in the different pieces of equipment are given in Table 2.3.

The uncertainties in thermophysical properties are not included in the table. For the OCR values, uncertainty propagation gave absolute uncertainty in the order of ±0.01 g, and so, two digits after the decimal point were shown for all the OCR values reported.

Table 2.2: Different sensors

Property/quantity	Instrument/sensor
Temperature	T-type thermocouples
Pressure	Absolute pressure transducers
Mass flow rate	Coriolis type flow meter
Oil concentration	Based on speed of sound

Table 2.3: Uncertainties of the different sensors

Instrument/sensor	Uncertainty
Thermocouple [°C]	±0.2
Pressure transducer [kPa]	±3.5
Mass flow meter [g/s]	±0.2%
Electronic mass balance [g]	±0.01

2.3 Flow visualization at compressor discharge

For flow visualization at the compressor discharge, a high-speed camera (2100 frames/second at a full resolution of 512 x 512 pixels) was used. The flow at the discharge provides qualitative evidence for the obtained OCR results. The discharge tube visualization setup is shown in Figure 2.8.

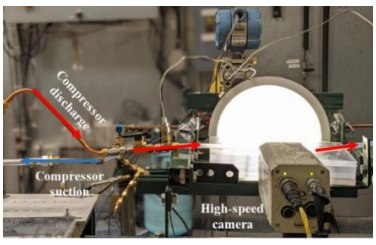

Figure 2.8: Flow visualization at the compressor discharge

CHAPTER 3: OCR MEASUREMENT AT LIQUID LINE

The method of OCR sampling involves taking a sample of refrigerant-oil mixture from the liquid line of the system, and then completely removing all the refrigerant from the sampling cylinder to leave just the oil inside. The oil concentration will be the ratio of the mass of oil to the total mass of the refrigerant-oil mixture entrapped within the cylinder where the mass of the dry sampling cylinder is M_1, the mass of the sampling cylinder with the sample of refrigerant-oil mixture is M_2, and the mass of the sampling cylinder containing just oil after the refrigerant has been removed is M_3. If the sample taken at the liquid line consists of only a single-phase homogeneous mixture of the refrigerant and the oil, and if the refrigerant-oil combination is miscible in the liquid phase, then the steady-state oil concentration measured from the mass analysis described above can be taken to be the OCR. The flow-chart for OCR sampling is provided in Figure 3.1. The OCR in the sample is calculated using Equation (3.1).

$$OCR = \frac{m_{oil}}{m_{oil} + m_{ref}} = \frac{M_3 - M_1}{M_2 - M_1} \tag{3.1}$$

All experiments were performed using a sampling cylinder with a valve-to-valve length of 8.5 inches and diameter of 3/8 inches. The dimensions were chosen based on the upper limit of the range of the mass scales that were used. Since the mass scales used for the present study had an upper limit of 500 g for the range, it had to be made sure that the total mass of the sampling cylinder and the entrapped sample was less than this value. Typical masses of refrigerant-oil mixtures entrapped inside the cylinders ranged between 18-22 g. The same sampling cylinders were used for all the different cases investigated in the present study.

To perform the oil sampling measurements, a bypass line was created after the condenser outlet, and the flow was diverted from the main line to the bypass line via a three-way valve. For

usual operation, the flow went through the main line, but when samples were taken, the flow was diverted to the bypass line which included the sampling cylinder. The sampling procedure used was the flow-through one, meaning that the flow of refrigerant-oil mixture was allowed to pass though the sampling cylinder, and once steady state was obtained, the valves on the sampling cylinder were closed, thus ensuring that the steady state mixture was captured. This is what was prescribed to be the best sampling procedure by Haider *et al.* [10]–[13].

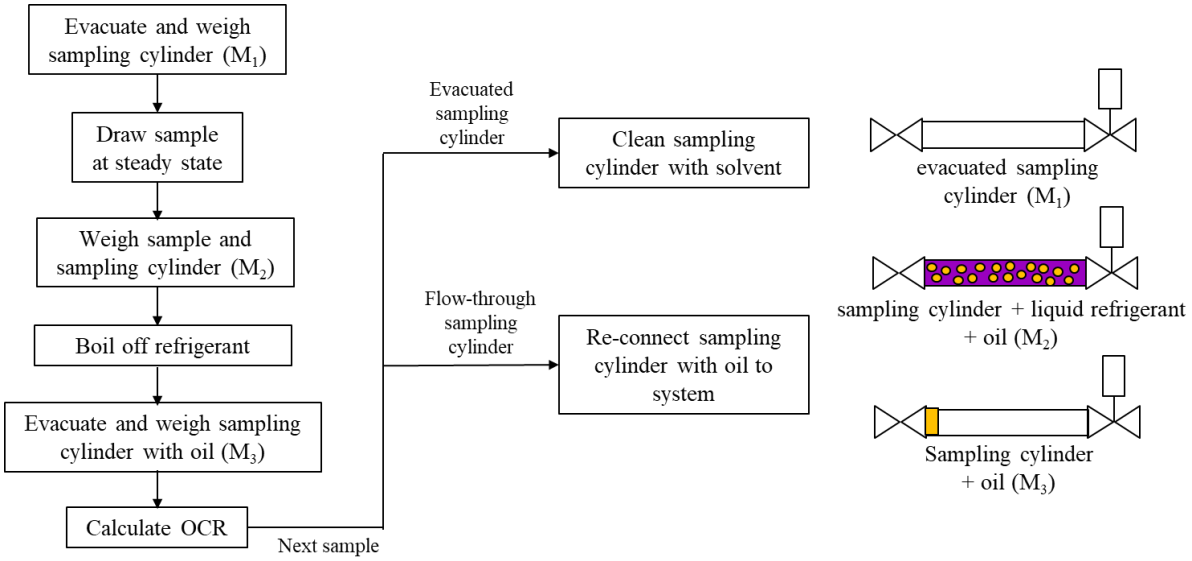

Figure 3.1: Flow-chart for OCR sampling

CHAPTER 4: RESULTS

4.1 Steady state data

Since the ASHRAE standard 41.4 (2015) requires the OCR measurement to be performed with the system in steady state, it had to be made sure that we learnt how to adjust system conditions to obtain steady state conditions. For steady state, we chose the AHRI A_{Full} conditions, which prescribes the indoor and outdoor air side temperatures (described in the previous chapter). The main challenge was to adjust the heaters, blowers and the cooling water circuit. Despite achieving the correct temperatures, we still encountered problems obtaining steady state result, and we later realized that it was due to the setting on the EEV. The EEV was initially set to automatic mode with the desired superheat set to 10°C, but this setting did not yield steady system conditions, there were always some fluctuations in the data. We suspected that it was due to the continuous adjustment of the stepper motor inside the expansion valve. So, we repeated the tests, and this time, we started with the EEV in automatic mode to find a rough estimate of the EEV open ratio for the 10°C superheat. Once this was obtained, we switched from the automatic mode to the manual mode and set the open ratio that was found during the automatic mode operation. This solved the problem and steady state was obtained for long periods. Figures 4.1-4.6 show the different steady state quantities that could be extracted from the data acquisition system.

All the steady state tests were performed for long periods to ensure that the system got enough time, and the refrigerant and air side temperatures could balance out. The data in the abovementioned figures were extracted for three different compressor speeds, and they were set to the VFD frequencies of 20 Hz, 25 Hz and 30 Hz. With a pulley ratio of 1.23, the compressor speeds came out to be 1437/min, 1798/min and 2155/min for the compressor model that we used.

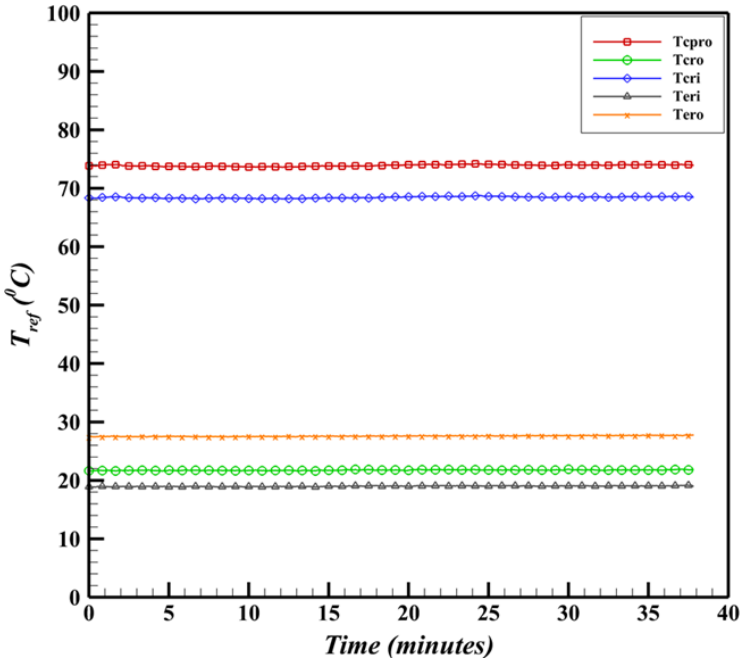

(a) Compressor speed = 1437/min

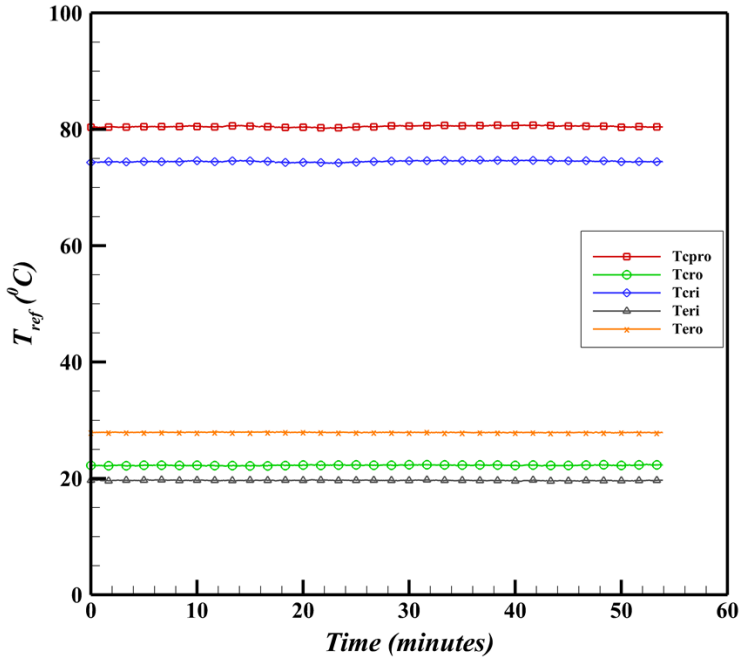

(b) Compressor speed = 1798/min

Figure 4.1: Refrigerant side temperatures at different compressor speeds

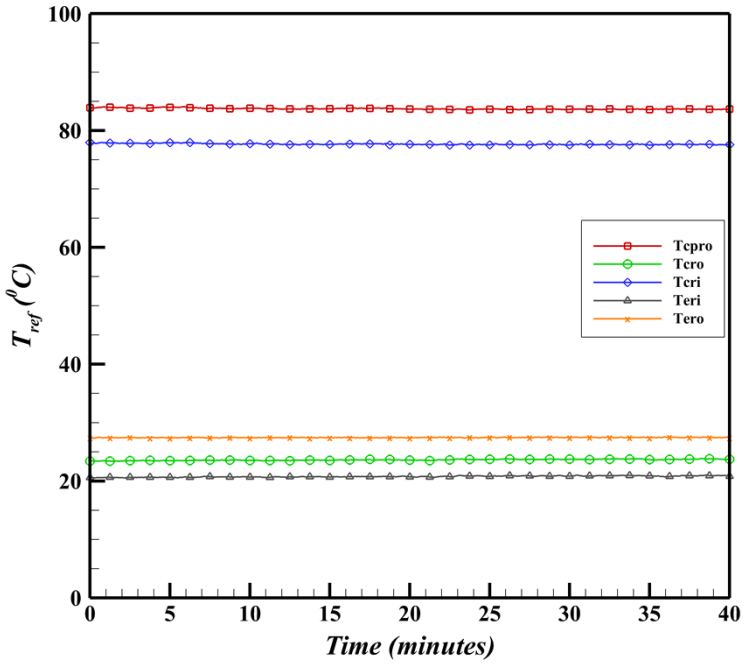

(c) Compressor speed = 2155/min

Figure 4.1: Refrigerant side temperatures at different compressor speeds (cont.)

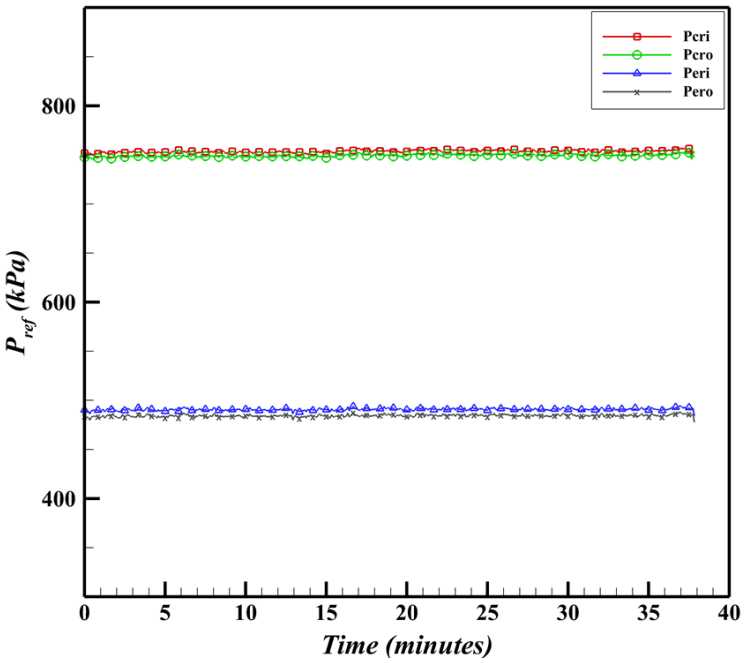

(a) Compressor speed = 1437/min

Figure 4.2: Refrigerant side pressures at different compressor speeds

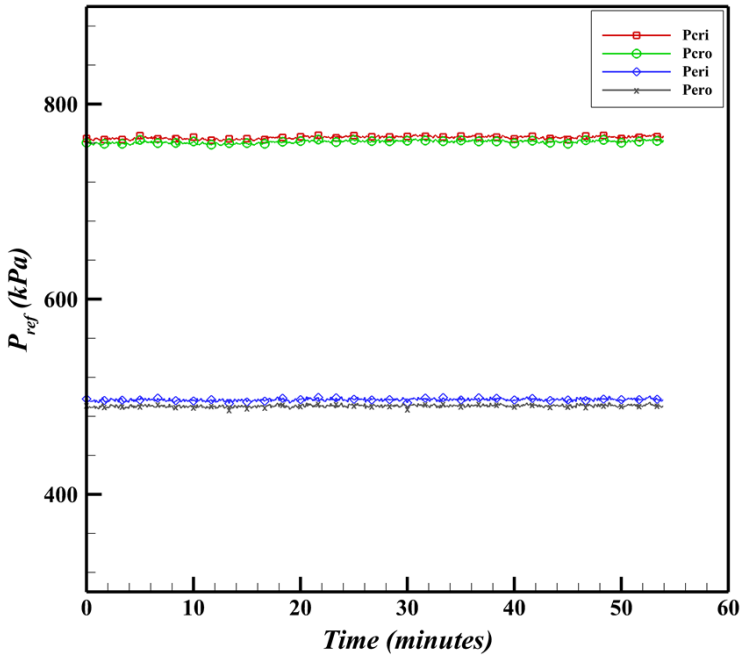

(b) Compressor speed = 1798/min

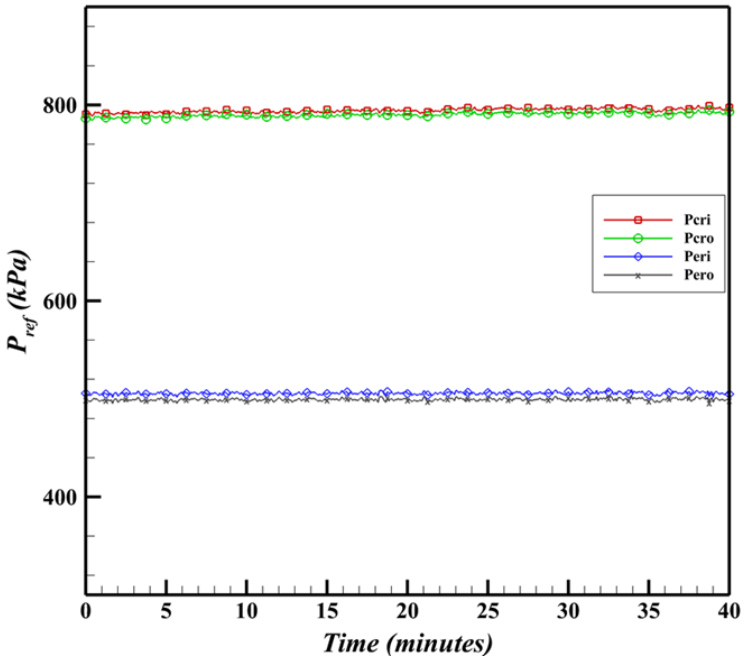

(c) Compressor speed = 2155/min

Figure 4.2: Refrigerant side pressures at different compressor speeds (cont.)

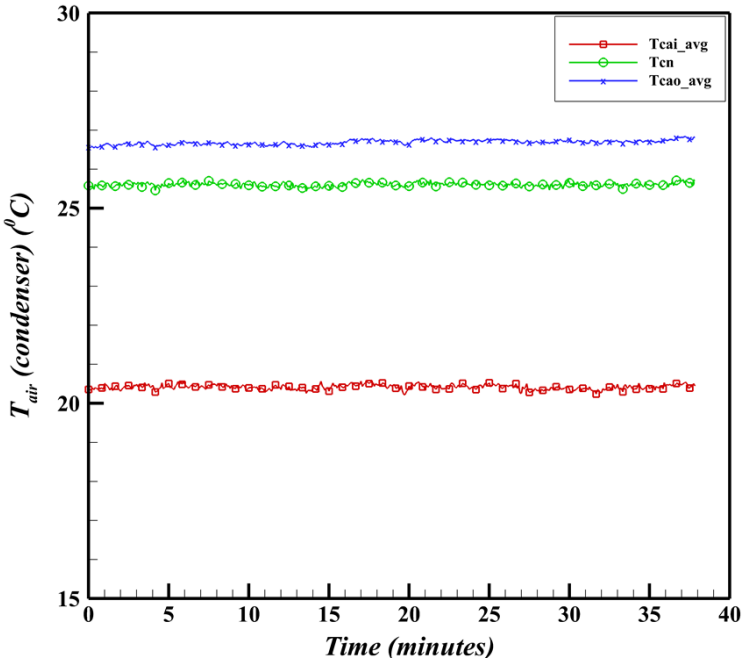

(a) Compressor speed = 1437/min

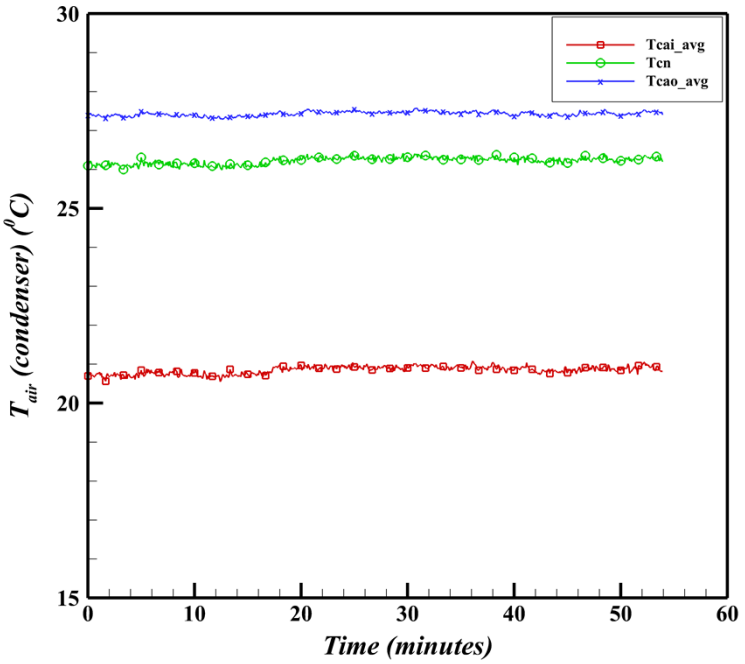

(b) Compressor speed = 1798/min

Figure 4.3: Condenser air side temperatures at different compressor speeds

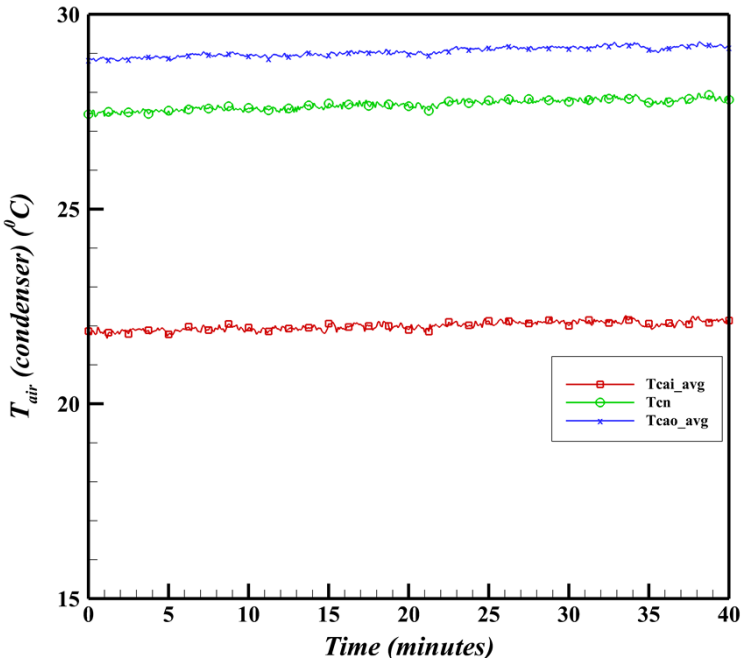

(c) Compressor speed = 2155/min

Figure 4.3: Condenser air side temperatures at different compressor speeds (cont.)

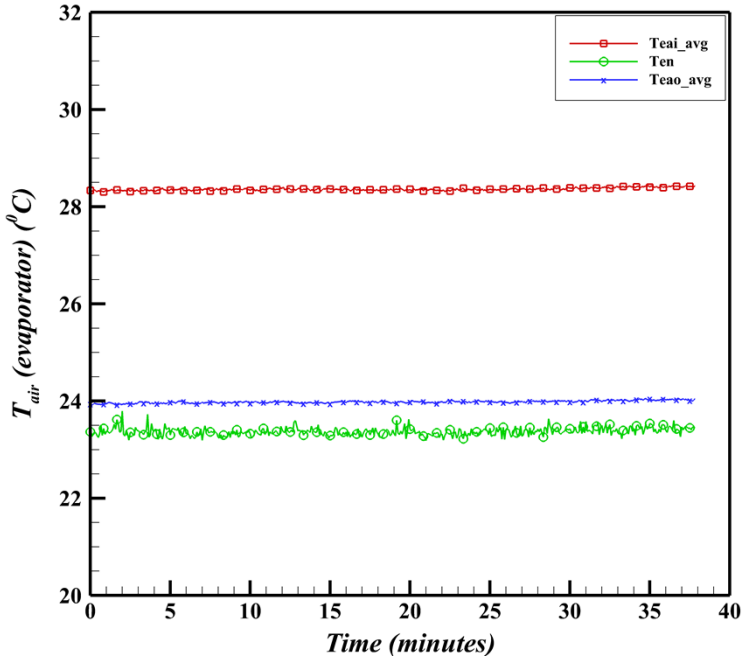

(a) Compressor speed = 1437/min

Figure 4.4: Evaporator air side temperatures at different compressor speeds

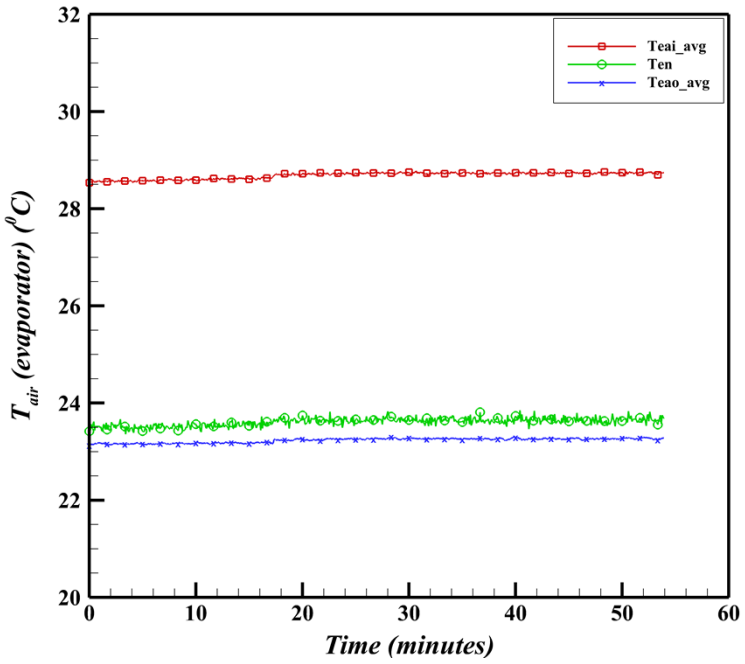

(b) Compressor speed = 1798/min

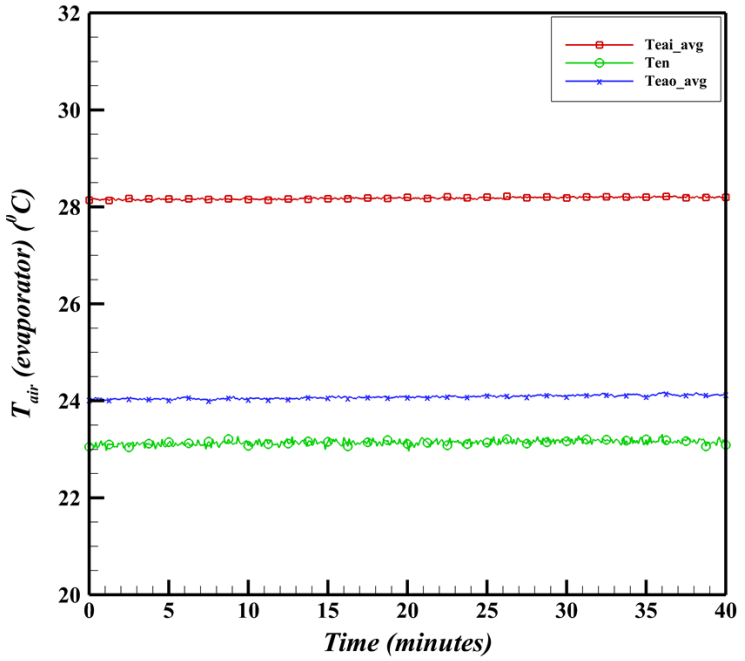

(c) Compressor speed = 2155/min

Figure 4.4: Evaporator air side temperatures at different compressor speeds (cont.)

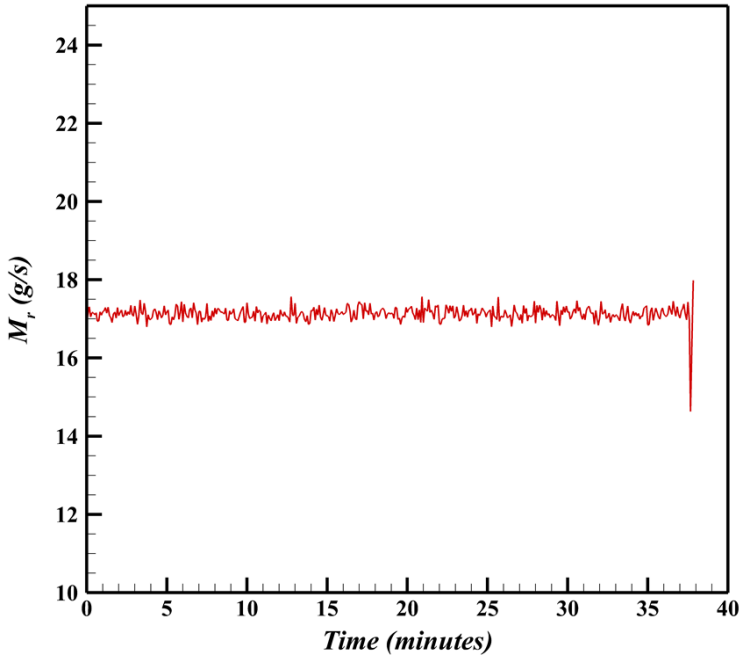

(a) Compressor speed = 1437/min

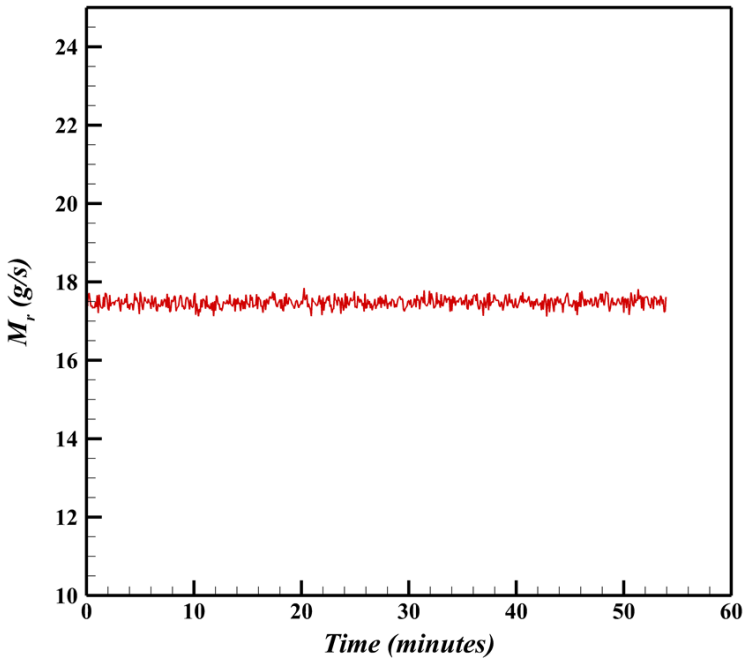

(b) Compressor speed = 1798/min

Figure 4.5: Refrigerant flow rates at different compressor speeds

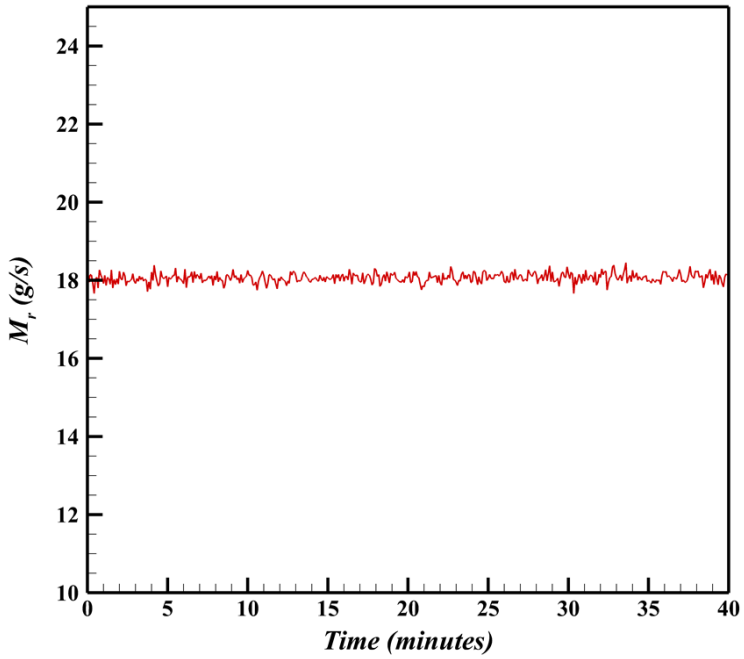

(c) Compressor speed = 2155/min

Figure 4.5: Refrigerant flow rates at different compressor speeds (cont.)

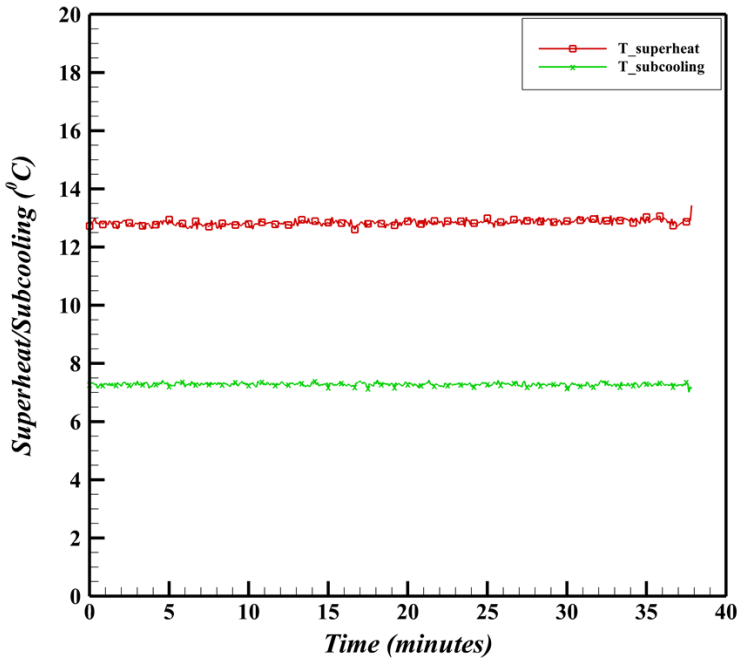

(a) Compressor speed = 1437/min

Figure 4.6: Refrigerant subcooling and superheat at different compressor speeds

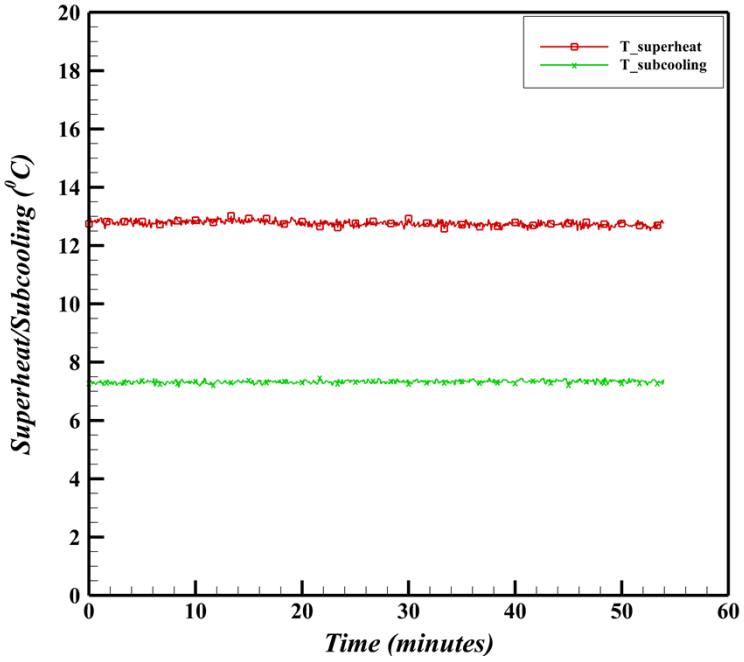

(b) Compressor speed = 1798/min

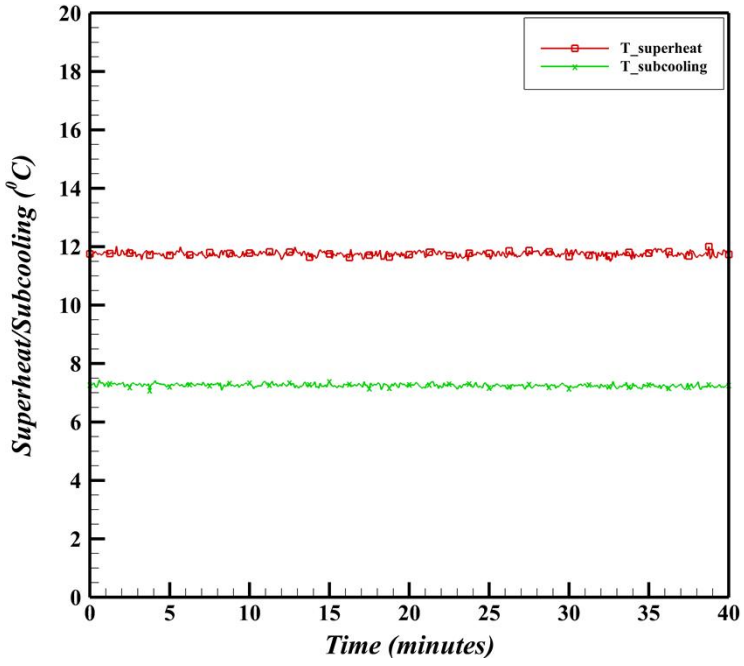

(c) Compressor speed = 2155/min

Figure 4.6: Refrigerant subcooling and superheat at different compressor speeds (cont.)

It can be seen in Figures 4.1-4.6 that all the different conditions for the system did indeed reach the steady state, and this allowed us to confirm that the system was capable of obtaining steady state, and hence, OCR measurements could be made properly.

4.2 OCR measurements

The technique used for OCR measurement was described in the previous chapter. The flow-through type sampling technique was adopted. Alongside sampling results, an oil concentration sensor based on speed of sound, (from Anton Parr) in the flowing fluid was also used as a guide to see if the trends matched. The steady state OCR data obtained from the speed of sound oil concentration sensor is provided in Figure 4.7. As can be seen from the real-time steady state data from the Anton Parr speed of sound sensor, the data were steady for sufficiently long periods. These results are then compared with sampling data performed at the liquid line.

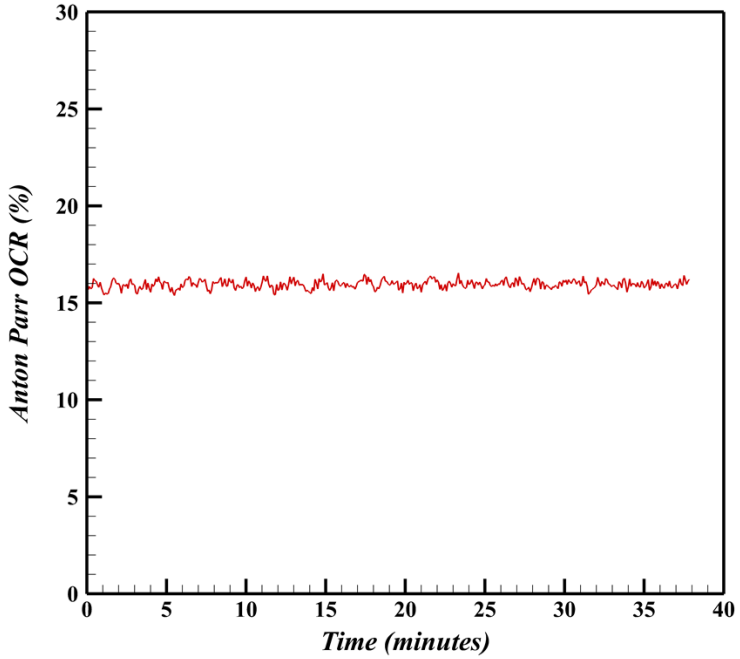

(a) Compressor speed = 1437/min

Figure 4.7: Oil concentration at different compressor speeds

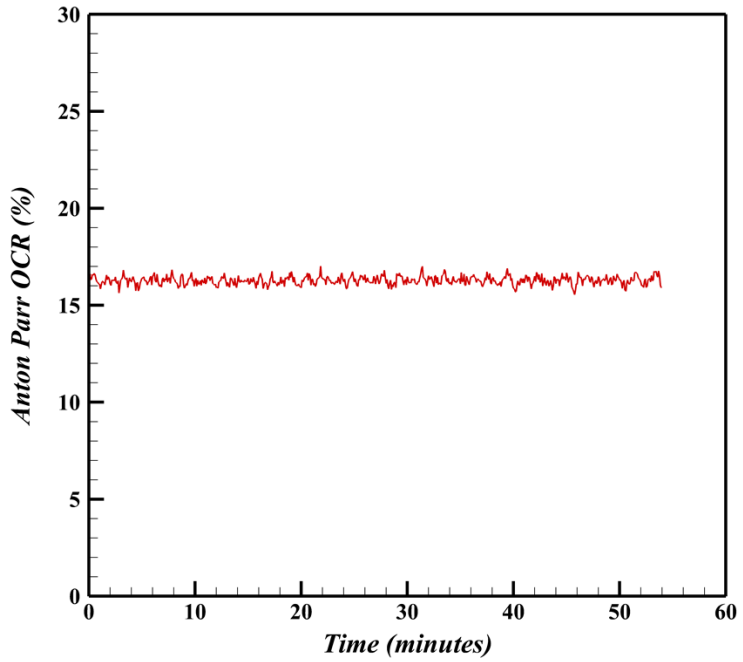

(b) Compressor speed = 1798/min

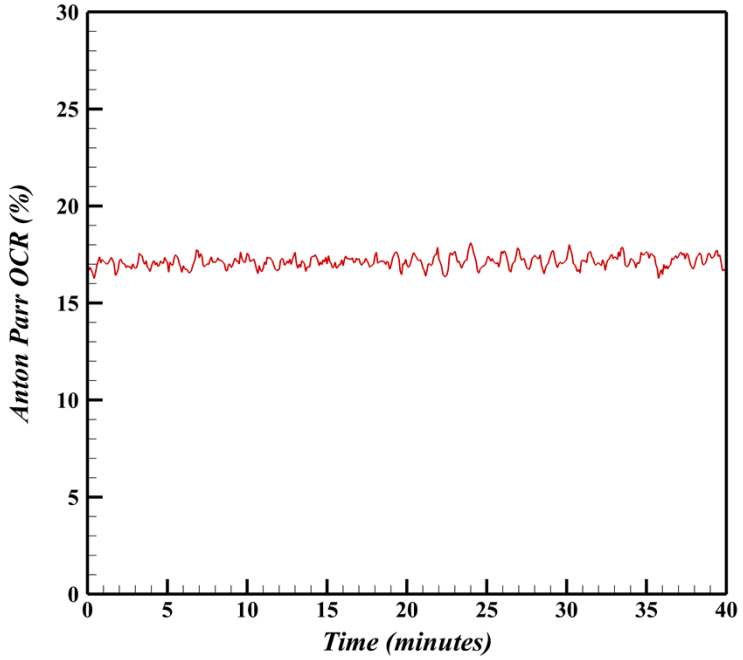

(c) Compressor speed = 2155/min

Figure 4.7: Oil concentration at different compressor speeds (cont.)

OCR was also measured using the sampling technique described by the ASHRAE standard 41.4 (2015). The difference from the standard is the fact that a flow-through type sampling cylinder was used as opposed to the evacuated type prescribed by the standard. But the whole process remains mostly the same. The OCR results, along with the steady state data obtained from the oil concentration sensor are given in Figure 4.8.

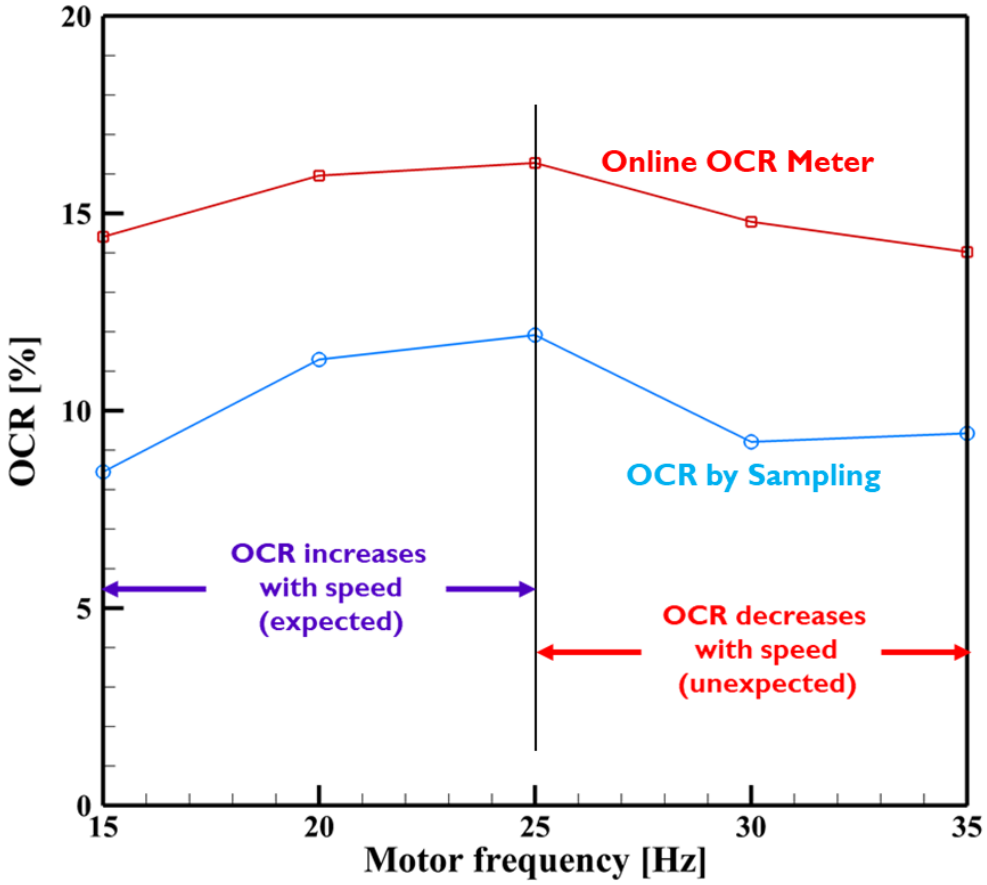

Figure 4.8: OCR results at different compressor speeds (pulley ratio = 1.23)

Figure 4.8 shows that with an increase in the compressor speeds, the OCR increases initially to reach a peak, but then at higher speeds, the OCR is seen to drop. This trend is common for results from both the oil concentration sensor and the sampling method. This result deviates

from what is expected: as the compressor spins at higher speeds, it is expected to pump out more oil, and hence, the OCR should also increase with the compressor speed.

We speculated that, at the higher compressor speeds (beyond the OCR peak), the compressor pumps out refrigerant at a higher flow rate, but the oil flow rate does not increase by the same degree. As a result, the calculated system OCR is lower. This can be a reasonable conclusion since the compressor speed and the mass flow rate are both closely related to the discharge and suction pressures of the compressor. At higher compressor speeds, and with refrigerant vapor occupying a much larger volume, it is possible that the oil flow rate cannot keep up with the refrigerant flow rate, thus resulting in the peak in OCR which was observed. This is an interesting observation and Ossorio and Navarro-Peris [24] and Ossorio et al. [25] obtained similar trends in OCR, but could not provide a clear explanation.

4.3 Flow visualization at compressor discharge

Xu and Hrnjak [5] devised a video-based method to predict the system OCR, and their method incorporated the visualization of the two phase flow of the refrigerant-oil mixture at the compressor discharge. They discussed how the two-phase flow at the compressor discharge consists of vapor refrigerant and liquid oil, flowing at different velocities. Depending on the compressor speed and the system conditions, and hence different OCRs, the flow patterns can look very different. At higher OCR cases, annular-mist flow is observed, where the oil flows as a film on the tube walls at a much smaller velocity compared to the higher velocity vapor core consisting of mostly vapor refrigerant, and tiny droplets of oil that get entrained by the refrigerant vapor. At lower OCR cases, the oil film on the tube walls breaks down into oil streams and droplets.

For the present work, a high-speed camera was used to observe the two-phase refrigerant-oil flow at the compressor discharge, and the images from the flow visualization are provided in Figure 4.9. The visualization for two different motor VFD frequencies of 25 Hz and 43 Hz, for the same pulley ratio of 1.23.

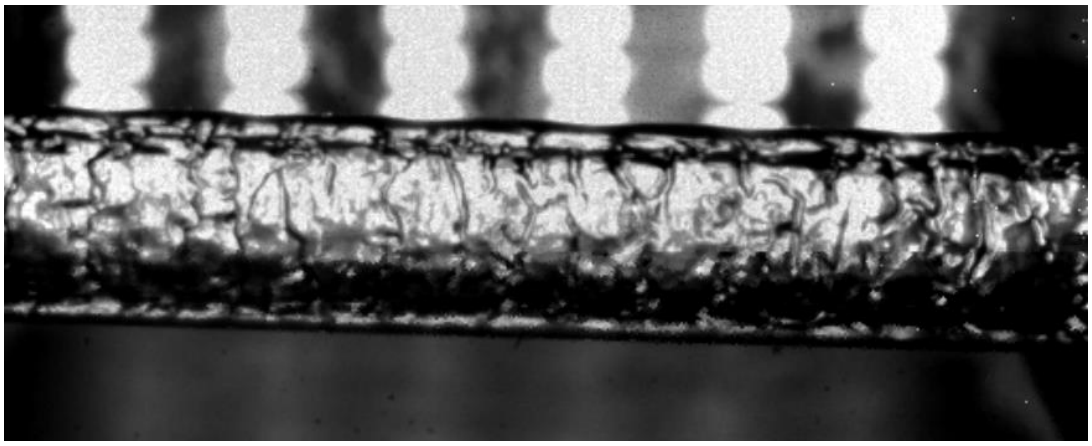

(a) Motor frequency = 25 Hz

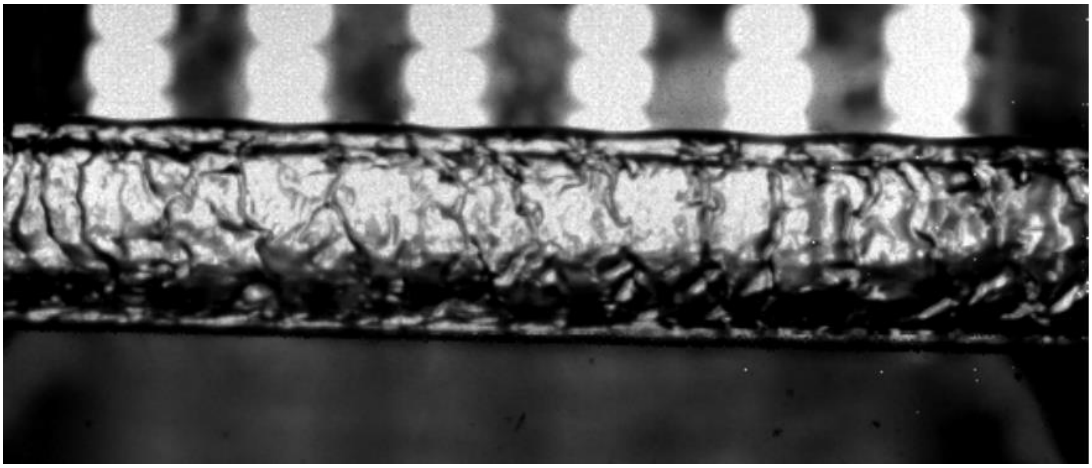

(b) Motor frequency = 43 Hz

Figure 4.9: Flow at discharge for two compressor speeds (pulley ratio = 1.23)

It is seen in Figure 4.9 that the flow at the compressor discharge for both the speeds investigated showed similar flow patterns. Both cases consisted of a wavy flow pattern on the tube walls. The waves were simply the oil film moving at much slower velocities compared to the vapor core. The flow at both the speeds were annular-mist flow in steady state. This indicates a higher OCR compared to flows with broken/unstable oil films and/or oil streams or droplets on the walls. It was difficult to draw solid conclusions about the OCR trends observed from the flow visualizations alone, and more analysis was necessary.

CHAPTER 5: CONCLUSIONS

Lubricant oil is essential in vapor compression systems because it helps to ensure that the useful life of the compressor is extended. It comes with a lot of beneficial effects, but most of these positive effects are limited to being within the compressor only. While the oil is ideally supposed to stay inside the compressor, it can mix with the refrigerant, leave the compressor, and make its way around the whole system and then back to the compressor in a process called oil circulation. However, not all of the oil that leaves the compressor returns to the compressor, some of it can get held up in different locations of the system in a process called oil retention. As a result, the oil content inside the compressor gradually decreases and it can even lead to compressor dry out and failure. Additionally, the oil mostly has negative effects on the rest of the system as it can lead to a decrease in cooling capacity and COP, leading to poor energy efficiency. So, it is very important to understand the effects of oil on the system, and one of the ways to do that is by taking a closer look at oil circulation within the whole system. The oil circulation rate (OCR) is the parameter that is most commonly used to quantify the degree of oil circulation.

The standard method of measuring the OCR in a system is described in the ASHRAE standard 41.4 (2015), and this is the method that is used across industry and academia to measure steady state OCR, and for the calibration of every other OCR measurement technique out there. The method is simple: it involved taking a sampling of refrigerant-oil mixture from the liquid line of the system, and the sample is then subjected to gravimetric analysis, and the OCR or oil concentration is calculated as the ratio of the mass of oil in the sample to the total mass of the refrigerant-oil mixture entrapped. In the present study, the same standard was followed for measuring the OCR, with the only difference being that the sampling technique used was the flow-

through type, instead of the evacuated type that is prescribed in the standard. Also, the sampling cylinders were made to be transparent so that complete filling up of the cylinders could be ensured.

The key objective of the current work was to first prepare an experimental facility which was out of commission for several years in a way that it could be used to run tests for a vapor compression system that could emulate a real automotive air conditioning system. This included connecting all the different components and learning how to use the heaters, blowers, and cooling water circuits in the environmental chambers to adjust the outdoor and indoor temperatures for the AC system. Once we mastered how to set the system conditions correctly, we started running the tests for OCR measurement in steady state.

The OCR was measured in steady state at different compressor speeds. It was observed that the OCR results reached a peak OCR and then dropped as the compressor speed increased. Although it was expected that with an increase in compressor speed, the OCR would keep increasing as the compressor would be sending out oil at a faster rate, that was certainly not the case. We speculated that the drop in OCR at higher compressor speeds was due to the refrigerant flow rate increasing much faster compared to the oil flow rate. Since the vapor refrigerant occupies more volume compared to the liquid oil, it is likely that the oil flow rate failed to keep up with the refrigerant flow rate, thus resulting in the drop in measured OCR.

The flow at the compressor discharge was visualized using a high-speed camera. In both the compressor speeds investigates, it was found that in steady state, the flow pattern observed was annular-mist flow, with a stable oil film on the tube wall. This is indicative of a higher OCR compared to flows with broken/unstable oil films and/or oil streams or droplets on the walls.

REFERENCES

[1] X. Wang, S. A. Haider, and S. Elbel, “Transient Oil Migration and Flow Behavior during Automotive Compressor Startup,” Warrendale, PA: SAE International, Apr. 2023. doi: 10.4271/2023-01-0142.

[2] X. Wang, S. A. Haider, and S. Elbel, “Oil Droplet vs. Film Flow at Discharge and Suction after Shutdown of Automotive Compressor,” Warrendale, PA: SAE International, Apr. 2023. doi: 10.4271/2023-01-0141.

[3] X. Wang, S. A. Haider, P. Hrnjak, and S. Elbel, “Transient Oil-refrigerant Mixture Migration and Change of Properties at Compressor Shutdown,” in *International Refrigeration and Air Conditioning Conference,* Jul. 2022. [Online]. Available: https://docs.lib.purdue.edu/iracc/2358

[4] X. Wang, S. A. Haider, P. Hrnjak, and S. Elbel, “Transient Migration of Oil at Compressor Discharge and Suction during Startup,” in *International Refrigeration and Air Conditioning Conference,* Jul. 2022. [Online]. Available: https://docs.lib.purdue.edu/iracc/2359

[5] J. Xu and P. Hrnjak, “Quantification of flow and retention of oil in compressor discharge pipe,” *International Journal of Refrigeration,* vol. 80, pp. 252–263, Aug. 2017, doi: 10.1016/j.ijrefrig.2017.05.004.

[6] R. Radermacher, L. Cremaschi, and R. A. Schwentker, “Modeling of Oil Retention in the Suction Line and Evaporator of Air-Conditioning Systems,” *HVAC&R Research,* vol. 12, no. 1, pp. 35–56, Jan. 2006, doi: 10.1080/10789669.2006.10391166.

[7] M. Youbi-Idrissi and J. Bonjour, “The effect of oil in refrigeration: Current research issues and critical review of thermodynamic aspects,” *International Journal of Refrigeration*, vol. 31, no. 2, pp. 165–179, Mar. 2008, doi: 10.1016/j.ijrefrig.2007.09.006.

[8] B. Shen and E. A. Groll, “Review Article: A Critical Review of the Influence of Lubricants on the Heat Transfer and Pressure Drop of Refrigerants, Part 1: Lubricant Influence on Pool and Flow Boiling,” *HVAC&R Research*, vol. 11, no. 3, pp. 341–359, Jul. 2005, doi: 10.1080/10789669.2005.10391142.

[9] X. Liu and P. Hrnjak, “Oil Effects On Performance Of Automobile A/C System,” in *International Refrigeration and Air Conditioning Conference*, Jan. 2016. [Online]. Available: https://docs.lib.purdue.edu/iracc/1648

[10] S. A. Haider, X. Wang, and S. Elbel, “Measurements of Oil Circulation Rate using Flow-through and Evacuated Type Sampling Cylinders for an Automotive Air Conditioning System,” Warrendale, PA: SAE International, Apr. 2023. doi: 10.4271/2023-01-0138.

[11] S. A. Haider, X. Wang, and S. Elbel, “Study of Flashing Flows Entering Evacuated Sampling Cylinders for Oil Circulation Rate Measurement in an Automotive Air Conditioning System,” Warrendale, PA: SAE International, Apr. 2023. doi: 10.4271/2023-01-0140.

[12] S. A. Haider, X. Wang, and S. Elbel, “Oil Circulation Rate Measurements with Flow-through and Evacuated Type Sampling Cylinders,” in *International Refrigeration and Air Conditioning Conference*, Jul. 2022. [Online]. Available: https://docs.lib.purdue.edu/iracc/2331

[13] S. A. Haider, X. Wang, and S. Elbel, “Effects of Orientation and Valve Opening Speed on Oil Circulation Rate Measurements Using an Evacuated Type Sampling Cylinder,” in *International Refrigeration and Air Conditioning Conference*, Jul. 2022. [Online]. Available: https://docs.lib.purdue.edu/iracc/2332

[14] S. Inampudi, F. Botticella, and S. Elbel, “Modeling and comparison of different capacity modulation strategies with focus on seasonal performance,” *IOP Conf. Ser.: Mater. Sci. Eng.*, vol. 1180, no. 1, p. 012039, Sep. 2021, doi: 10.1088/1757-899X/1180/1/012039.

[15] S. T. Inampudi, F. Botticella, and S. Elbel, “Comparative Experimental Analysis Of Different Compressor Capacity Modulation Strategies In R410A Chiller With Focus On Seasonal Performance,” *International Compressor Engineering Conference*, Jan. 2022, [Online]. Available: https://docs.lib.purdue.edu/icec/2729

[16] S. Inampudi, F. Botticella, and S. Elbel, “Part load performance of single and two stage compressors — a comparative experimental study in a R410A chiller unit,” *IOP Conf. Ser.: Mater. Sci. Eng.*, vol. 1180, no. 1, p. 012050, Sep. 2021, doi: 10.1088/1757-899X/1180/1/012050.

[17] S. Inampudi, F. Botticella, and S. Elbel, “Experimental Comparison Of Seasonal Performance In R410A Chiller Using Single Speed And Two Stage Compressor,” in *International Compressor Engineering Conference*, May 2021. [Online]. Available: https://docs.lib.purdue.edu/icec/2684

[18] S. T. Inampudi and S. Elbel, “Study Of Charge Optimization And Compressor Modulation Strategies Effect On The Seasonal Performance In A R410A Chiller,” in *International Compressor Engineering Conference*, Jan. 2022. [Online]. Available: https://docs.lib.purdue.edu/icec/2730

[19] C. Tian, Y. Liao, and X. Li, “A mathematical model of variable displacement swash plate compressor for automotive air conditioning system,” *International Journal of Refrigeration*, vol. 29, no. 2, pp. 270–280, Mar. 2006, doi: 10.1016/j.ijrefrig.2005.05.002.

[20] S. Kim and P. Hrnjak, “Effect of Oil on Flow Boiling Heat Transfer and Flow Patterns of CO2 in 11.2 mm Horizontal Smooth and Enhanced Tube,” in *International Refrigeration and Air Conditioning Conference*, Jan. 2012. [Online]. Available: https://docs.lib.purdue.edu/iracc/1331

[21] H. Li and P. Hrnjak, “An experimentally validated model for microchannel heat exchanger incorporating lubricant effect,” *International Journal of Refrigeration*, vol. 59, pp. 259–268, Nov. 2015, doi: 10.1016/j.ijrefrig.2015.07.020.

[22] J. Zhu, F. Botticella, and S. Elbel, “Experimental investigation and theoretical analysis of oil circulation rates in ejector cooling cycles,” *Energy*, vol. 157, pp. 718–733, Aug. 2018, doi: 10.1016/j.energy.2018.05.152.

[23] F. Siddiqui, “A Study of Cross-Flow Air Heating via a Multiport Serpentine Microchannel Heat Exchanger.”

[24] R. Ossorio and E. Navarro-Peris, “Study of oil circulation rate in variable speed scroll compressor working with propane,” *International Journal of Refrigeration*, vol. 123, pp. 63–71, Mar. 2021, doi: 10.1016/j.ijrefrig.2020.12.002.

[25] R. Ossorio, E. Navarro-Peris, and R. B. Barta, “Impact of lubricant in the performance of variable speed heat pumps working with R290,” *International Journal of Refrigeration*, vol. 145, pp. 436–445, Jan. 2023, doi: 10.1016/j.ijrefrig.2022.10.003.

APPENDIX A: EES CODE FOR SAMPLE SYSTEM CALCULATIONS

```
"Compressor speed = 1500 RPM"
"@AHRI A_full Condition (T_cai = 35C (90F), T_eai = 26.67C (80F))"

speed_RPM = 1500
disp_V = 2.4 * 10^(-5)

"Refrigerant side temperature"
T[1] = 57.3 "Tcpro"
T[2] = 54.0 "Tcri"
T[3] = 36.7 "Tcro"
T[4] = 17.8 "Teri"
T[5] = 26.4 "Tero"
T[6] = 25.1 "Tcpri"
T[7] = T[1]

Tcpro = T[1]
Tcri = T[2]
Tcro = T[3]
Teri = T[4]
Tero = T[5]
Tcpri = T[6]

"Refrigerant side pressure"
P[1] = 1008 "Pcpro"
P[2] = 1008 "Pcri"
P[3]= 1004 "Pcro"
P[4] = 519.7 "Peri"
P[5] = 514.9 "Pero"
P[6] = 460.3 "Pcpri"
P[7] = P[1]

Pcpro = P[1]
Pcri = P[2]
Pcro = P[3]
Peri = P[4]
Pero = P[5]
Pcpri = P[6]

"Air side temperature"
Tcai_avg = 35.2
Tcao_avg = 38.2
Teai_avg = 27.1
Teao_avg = 24.1
```

"Mass flow rate of oil-refrigerant mixture"
mr=0.01146

"Calculated enthalpies"
h[1] = enthalpy(R134a , T = T[1] , P = P[1])
h[2] = enthalpy(R134a , T = T[2] , P = P[2])
h[3] = enthalpy(R134a , T = T[3] , P = P[3])
h[4] = h[3]
h[5] = enthalpy(R134a , T = T[5] , P = P[5])
h[6] = enthalpy(R134a , T = T[6] , P = P[6])
h[7] = h[1]

hcpro = h[1]
hcri = h[2]
hcro = h[3]
heri = h[4]
hero = h[5]
hcpri = h[6]

"Air side capacities from program"
Q_ea = 1.46
Q_ca = 2.41

"System calculations"
Pressure_ratio = P[2] / P[6]

Tero_sat = t_sat(R134a, P=P[5])
Tsup = T[5] - Tero_sat

Tcro_sat = t_sat(R134a, P=P[3])
Tsub = Tcro_sat - T[3]

Q_c = mr * (hcpro - hcro)
Q_e = mr * (hero - heri)

COP = (hero - heri) / (hcpro - hero)

s1 = entropy(R134a, T = T[6], P = P[6])
h2s = enthalpy(R134a, s = s1, P = P[2])

ETA_c = (h2s - hero) / (hcpro - hero)

rho_suct = density(R134a, T = T[6], P = P[6])
ETA_v = mr / (rho_suct * (speed_RPM / 60) * disp_V)

APPENDIX B: P-H DIAGRAM FOR SYSTEM IN STEADY STATE